Discover Oncology

Analysis

Unraveling molecular signatures and prognostic biomarkers in glioblastoma: a comprehensive study on treatment resistance and personalized strategies

Jinmin Xue[1,2] · **Jie Zhang**[1,2] · **Jing Zhu**[1,2,3]

Received: 21 July 2024 / Accepted: 28 November 2024
Published online: 04 December 2024
© The Author(s) 2024 OPEN

Abstract

Background Glioblastoma (GBM) is a highly aggressive primary brain tumor with limited treatment success and poor prognosis. Despite surgical resection and adjuvant therapies, GBM often recurs, and resistance to radiotherapy and temozolomide presents significant challenges. This study aimed to elucidate molecular signatures associated with treatment responses, identify potential biomarkers, and enhance personalized treatment strategies for GBM.

Methods We conducted a comprehensive analysis using the Gene Expression Omnibus (GEO) and The Cancer Genome Atlas (TCGA) databases. The GEO dataset (GSE206225) was used to identify differentially expressed genes (DEGs) between radiation-sensitive/resistant and temozolomide-sensitive/resistant GBM samples. TCGA data were utilized for subsequent analyses, including Lasso-Cox regression, risk score model construction, Kaplan–Meier survival analysis, and gene set enrichment analysis (GSEA). Hub genes were identified through survival analysis, and a gene prognostic nomogram was developed. Additionally, validation of the three-gene risk signature through multiple external cohorts and validation of protein expression levels were performed.

Results DEG analysis identified 111 genes associated with chemoradiotherapy resistance, providing insights into the complex landscape of GBM treatment response. The risk score model effectively stratified patients, showing significant differences in overall survival and progression-free survival. GSEA offered a deeper understanding of pathway activities, emphasizing the intricate molecular mechanisms involved. NNAT, IGFBP6, and CYGB were identified as hub genes, and a gene prognostic nomogram demonstrated predictive accuracy.

Conclusion This study sheds light on the molecular intricacies governing GBM treatment response. The identified hub genes and the gene prognostic nomogram offer valuable tools for predicting patient outcomes and guiding personalized treatment strategies. These findings contribute to advancing our understanding of GBM biology and may pave the way for improved clinical management.

Keywords Glioblastoma · Radiotherapy resistance · Chemotherapy resistance · Differentially expressed genes · Prognostic biomarkers · Immune microenvironment

Supplementary Information The online version contains supplementary material available at https://doi.org/10.1007/s12672-024-01649-y.

✉ Jing Zhu, 22118731@qq.com; Jinmin Xue, xuejinmin@163.com; Jie Zhang, 204377@cqmu.edu.cn | [1]Department of Oncology, The First Affiliated Hospital of Chongqing Medical University, Chongqing 400000, China. [2]Department of Oncology, Jinshan Hospital of the First Affiliated Hospital of Chongqing Medical University, Chongqing 400016, China. [3]Division of General and Gastrointestinal Surgery, Department of Surgery, Massachusetts General Hospital, Harvard Medical School, Boston, MA 02114, USA.

1 Introduction

Glioblastoma (GBM) is the most common and highly aggressive primary brain tumor, classified as grade IV by the World Health Organization (WHO) due to its characteristic histopathological features, including necrosis and endothelial proliferation [1]. In 2010, approximately 138,054 individuals in the United States were diagnosed with a primary malignant brain tumor, with malignant gliomas being the predominant subtype, accounting for 80% of cases and approximately 17,000 new diagnoses annually. GBM predominantly affects individuals aged 60 to 80, and its prevalence is expected to rise with an aging population [2, 3].

The etiology of GBM remains largely unknown for most patients. Approximately 5% of individuals carry germline mutations that predispose them to various tumor types, including GBM [4, 5]. In addition, a small subset of patients has a family history of cancer. Ionizing radiation is the primary established risk factor for GBM, though only a minority of radiation-induced cranial tumors progress to GBM [6, 7]. Other potential factors, including exposure to cell phones, viral triggers (such as cytomegalovirus), and other environmental exposures, are under investigation, but their roles remain unclear [8–12].

Currently, there are no early detection methods for GBM. Magnetic resonance imaging (MRI) remains the most sensitive diagnostic tool; however, by the time a lesion is detectable by MRI, the tumor has typically reached an advanced stage [13].

The standard treatment for newly diagnosed GBM patients includes maximal surgical resection followed by field radiotherapy combined with temozolomide chemotherapy for up to six maintenance cycles [14–16]. Despite these interventions, local recurrence is almost inevitable [17]. largely due to the genetic heterogeneity of GBM, the blood–brain barrier (BBB), and an immunosuppressive tumor microenvironment [18].

Resistance to radiotherapy is thought to be a significant contributor to the high mortality rate of GBM. The underlying causes of radioresistance are complex and multifactorial, often associated with recurrence. Similarly, temozolomide resistance is a major obstacle in GBM treatment, and the mechanisms driving this resistance are not yet fully understood. Current research focuses on elucidating the molecular pathways involved in therapy resistance, particularly alterations in signal transduction pathways that drive tumor resilience [19]. Despite these efforts, GBM remains an incurable disease, with a poor prognosis. The median survival rate for patients is between 12 and 15 months, with only 2.3% surviving beyond 2 years and 1.2% beyond 3 years, even for younger patients in good health [20].

GBM's aggressive nature presents substantial challenges for prognosis and treatment response. Identifying which patients would benefit most from radiotherapy and temozolomide remains difficult. A deeper understanding of the molecular mechanisms governing the responses to these therapies is critical for advancing personalized treatment strategies. In this context, we conducted a comprehensive analysis of differentially expressed genes (DEGs) in radiation-sensitive and temozolomide-sensitive GBM samples. Our goal was to identify specific biomarkers that could predict therapeutic sensitivity and elucidate the molecular signatures associated with treatment response.

2 Methods

2.1 Overview

To provide a clear understanding of our comprehensive research process, we have included a detailed workflow table (Table 1). This table outlines each critical step of our study, from data collection to validation, including the specific tools and methodologies used. The table serves as a guide to the systematic approach taken to identify molecular signatures, construct prognostic models, and validate findings within different cohorts.

2.2 Project selection and data collection

The data for this study were acquired from Gene Expression Ominibus, a public functional genomics data repository. Considering "glioblastoma", "radiation", and "resistance" as three key words for obtaining desired project, we ultimately enrolled series GSE206225 as our main dataset to analyze [21]. The overall goal of this project was to determine if there were baseline differences between patient-matched primary and recurrent tumors following serial radiation treatment. The tissues were categorized into "Radiation sensitive" and "Radiation resistant" groups and further stratified into

Table 1 Detailed workflow table for glioblastoma (GBM) prognostic model construction and analysis

Step	Details	Purpose	Tools/databases
1. Data collection	Acquire data from GEO and TCGA databases related to GBM Keywords used: "glioblastoma", "radiation", "resistance"	Collect sufficient gene expression and clinical information for subsequent analysis	GEO Database (GSE206225), TCGA Database
2. Identification of differentially expressed genes (DEGs)	Use GEO2R to analyze DEGs between radiation-sensitive/resistant and temozolomide-sensitive/resistant samples (criteria: $P < 0.05$, $logFC > 1$) Use a Venn diagram to identify common DEGs between the groups	Identify specific genes related to treatment response	GEO2R, Venn Diagram
3. Functional enrichment analysis	Perform enrichment analysis of the identified DEGs using Metascape Identify pathways such as interferon signaling, system regulation, and cellular export	Understand the function of DEGs and their role in GBM treatment	Metascape (https://metascape.org)
4. Lasso-Cox regression model construction	Perform Lasso-Cox regression to optimize the predictive model and eliminate gene collinearity Extract 8 key genes and calculate the risk score	Build a risk score model to predict GBM prognosis	R (glmnet package, tenfold cross-validation)
5. Risk score calculation and patient stratification	Calculate risk scores using the Lasso-Cox model, stratifying patients into high-risk and low-risk groups based on median values Perform survival difference analysis	Stratify patients by gene expression to assess prognosis	Kaplan–Meier survival analysis, Log-Rank Test
6. Survival analysis and GSEA	Perform Kaplan–Meier analysis for Overall Survival (OS) and Progression-Free Interval (PFI) between high and low-risk groups Conduct GSEA to analyze differential pathway activity (e.g., adhesion, chemokine signaling)	Understand biological differences between risk groups	R (survival package, survminer package), GSEA
7. Identification of hub genes	Identify 3 hub genes (NNAT, IGFBP6, CYGB) based on survival analysis Use univariate Cox regression analysis to determine gene association with survival	Identify key genes significantly impacting prognosis	Kaplan–Meier survival analysis, Cox Regression
8. Construction of prognostic nomogram	Integrate hub genes with clinical parameters (age, sex, IDH mutation status, Karnofsky Performance Score) to construct a prognostic nomogram	Provide a personalized prognosis prediction tool	R (rms package, forestplot package)
9. Validation with external datasets	Validate the accuracy of the three-gene risk signature using multiple independent external datasets Perform z-score normalization and apply exponential transformation	Validate the robustness and applicability of the model in different patient groups	External Independent Datasets, R
10. Protein expression validation	Download immunohistochemistry (IHC) data from the Human Protein Atlas (HPA) to verify protein expression levels of the hub genes in GBM and normal tissues	Confirm consistency between gene expression and protein levels	HPA (https://www.proteinatlas.org)

"Temozolomide sensitive" and "Temozolomide resistant" groups. We employed GEO2R to analyze differentially expressed genes (DEGs) between these groups. Additionally, we used Metascape (http://www.metascape.org/) to determine gene functions and pathways associated with the identified DEGs.

2.3 Standard Cox regression analysis and prognostic model construction

The survival package was used for proportional hazards testing and standard Cox regression, while rms supported model construction and validation. Data were obtained from the TCGA-GBM project within the TCGA database, with RNA-seq data processed to TPM format alongside relevant clinical information. Additional variables, including WHO grade, IDH mutation status, and 1p/19q codeletion, were incorporated. Normal samples and those lacking clinical information were excluded, and TPM data were log2-transformed (log2(value + 1)) for standardization. In univariate Cox regression, variables meeting a specified P-value threshold were selected and included in the multivariate Cox model to assess independent prognostic significance for overall survival (OS).

2.4 LASSO-Cox regression analysis and construction of prognostic prediction mode

We used The Cancer Genome Atlas (TCGA) database to assemble the training cohort for GBM patients based on gene expression data and relevant clinical information. Analysis was conducted on 166 GBM cases with complete follow-up data, excluding cases with incomplete survival data. A Lasso-Cox regression analysis was used to refine the model and eliminate collinearities among radiation/temozolomide resistance genes. This analysis was conducted using the "glmnet" package, where the Cox penalty regression was implemented through the glmnet function, and tenfold cross-validation was executed with the cv.glmnet function [22, 23].

The penalization parameter was determined by assessing the minimum log-likelihood deviation through tenfold cross-validation in the metadata set, corresponding to the optimal λ value. With the specified λ, coefficients (Coef) for each feature were extracted, leading to the formulation of a risk score model. This model entailed multiplying the β (Coef) values with the expression levels of drug resistance-related genes (GRPGs): Risk score = (β1 * GRPG1 + β2 * GRPG2 + β3 * GRPG3 + ⋯ + βn * GRPGn), where β represents the coefficients of GRPGs.

Based on the median risk score values, the 166 patients were classified into high-risk and low-risk groups using the risk score model. With the "survival" package and the "survminer" package, Kaplan–Meier survival analysis and log-rank tests were performed on these groups. This allowed for the elucidation of differences in overall survival (OS) and Progression Free Interval (PFI). As a consequence of this comprehensive approach, it was possible to analyze OS and PFI disparities with a high degree of accuracy compared to low-risk groups.

2.5 Gene set enrichment analysis (GSEA) and gene set variation analysis (GSVA)

To comprehensively examine differential pathway activity between high-risk and low-risk groups, we used Gene Set Enrichment Analysis (GSEA). Six gene sets from the MSigDB database and tumor-specific gene sets from the CancerSEA study were utilized for enrichment analysis. The expression matrix representing the relationship between samples and genes was transformed using the GSVA package. This transformation converted the original "sample × gene" matrix into a "sample × pathway" matrix, directly reflecting associations between samples and pathways.

We then performed differential analysis using the limma package to identify pathways with significant differences between samples. By integrating GSEA and differential pathway analysis, we sought to reveal the intricate landscape of pathway activities associated with risk stratification, providing valuable insights into potential molecular mechanisms that contribute to the observed differences in OS and PFI.

2.6 Identifcation of hub genes by Kaplan–Meier survival analysis

Following guidelines and policies (http://portal.gdc.cancer.gov/), we collected raw counts of RNA-sequencing data and corresponding clinical information from the TCGA GBM dataset. To compare survival differences between the groups, Kaplan–Meier survival analysis with log-rank tests was conducted. Univariate Cox proportional hazards regression analysis was used to calculate p-values, hazards ratios (HR), and Kaplan–Meier curves based on 95% confidence intervals (CIs). It was found that three genes, NNAT, IGFBP6, and CYGB, significantly correlated with survival time.

2.7 Expression analysis and correlation analysis

To analyze the molecular differences between two distinct groups within the TCGA glioma database, we utilized the Mann–Whitney U test (also known as the Wilcoxon rank sum test). Based on RNA-sequencing expression profiles and clinical information for GBM from TCGA (https://portal.gdc.cancer.gov), expression and correlation analyses were conducted. A two-gene correlation map was generated using the R software package ggstatsplot. Spearman's correlation analysis, a robust non-parametric statistical approach, was applied to describe correlations between quantitative variables that did not follow a normal distribution.

2.8 Analysis of immune cell infiltration on hub genes

The methodology for immune infiltration analysis utilized the TISIDB (Tumor Immune Single-cell Database) website. Initially, relevant immune infiltration information for tumor samples was retrieved, encompassing the relative abundance of various immune cell types and associated immune gene expression data. Through the TISIDB user interface, the target tumor type and relevant parameters were selected to obtain desired immune infiltration results, including proportions of different immune cell subtypes and expression levels of immune-related genes.

2.9 The protein–protein interaction (PPI) analysis

The PPI analysis and gene enrichment analysis were conducted using the String database (https://string-db.org/). The initial query of the database involved a list of genes or proteins of interest. String provided a comprehensive PPI network by integrating known and predicted protein interaction information. To ensure result reliability, high-confidence PPIs were selected by setting specific confidence score thresholds. Subsequent gene enrichment analysis utilized various public databases and annotation resources, including Gene Ontology (GO) annotations, Kyoto Encyclopedia of Genes and Genomes (KEGG) pathways, biological processes, molecular functions, among others. This approach provided insights into the functional and pathway-level implications within the list of genes or proteins of interest.

2.10 Construction of nomogram with hub genes and development of calibration curves to predict the outcome of GBM

To construct the nomogram predicting overall recurrence, univariate and multivariate Cox regression analyses were conducted using RNA-sequencing expression profiles, along with corresponding clinical information for GBM from the TCGA dataset. A forest plot is generated using the R package 'forestplot', which displays P values, HRs, and the 95% CIs. Subsequently, a nomogram was developed based on the multivariate Cox proportional hazards analysis results to estimate X-year overall recurrence. The nomogram visually represented contributing factors, allowing clinicians to calculate an individual patient's recurrence risk by assigning points associated with each risk factor. This was implemented using the 'rms' R package, offering a user-friendly tool for personalized risk assessment and communication for GBM patients.

2.11 Validation of the three-gene risk signature through multiple external cohorts

We performed z-score normalization on all datasets to standardize the data and applied an exponential function to adjust for non-negativity and interpretability in risk assessment. After data preprocessing, risk scores for each sample were calculated using risk coefficients derived from the training set by the Lasso-Cox method.

To validate the three-gene risk signature, we used multiple independent external datasets (For example, GEO, CGGA datasets, etc.). The results consistently indicated that the high expression group was associated with poorer prognosis, demonstrating the robustness and reproducibility of the proposed risk signature across diverse cohorts.

2.12 Validation of the protein expression levels of the hub genes via the human protein atlas

An immunohistochemistry (IHC) analysis was performed based on data downloaded from the Human Protein Atlas (HPA, http://www.proteinatlas.org) in order to verify the protein expression levels in GBM and normal tissues. IHC results could be obtained for a number of proteins based on proteomics in normal and cancer tissues by HPA.

2.13 Statistical analysis

All the analysis methods and R package were implemented by R version 4.0.3. Group comparisons were performed utilizing the Wilcoxon test. A significance level of $P < 0.05$ was considered statistically significant.

3 Results

3.1 Analysis of differentially expressed genes (DEGs) in radiation-sensitive and temozolomide-sensitive samples in a GBM cohort and their functional enrichment

We analyzed DEGs using the GEO dataset GSE206225 with GEO2R. Our findings revealed 319 DEGs between radiation-sensitive and radiation-resistant groups and 1197 DEGs between temozolomide-sensitive and temozolomide-resistant groups in GBM, meeting the criteria of $P < 0.05$ and $logFC > 1$.

Figure 1A and B present volcano plots and heatmaps of these DEGs, respectively. Comprehensive lists of upregulated and downregulated genes are provided in Additional file 1: Tables S1 and S2. Using a Venn diagram, we identified 111 overlapping DEGs between both groups (Fig. 1C). Further functional and pathway enrichment analysis of these DEGs using Metascape revealed significant enrichment in pathways such as interferon signaling, interferon-gamma signaling, regulation of system processes, and cell export (Fig. 1D).

3.2 Prediction model built based on Lasso-Cox regression

The clinical summary of the training cohort for GBM patients in the TCGA database is presented in Table S3. The TCGA GBM cohort had an average patient age of 59.4 years (range 21–89), with a predominance of males (107) over females (59). Racially, the cohort was primarily White (148), with smaller groups identifying as Black or African American (11) and Asian (7). Survival analysis showed that 133 patients were deceased at the study's conclusion, with a median overall survival (OS) of 373 days. Disease progression was documented in 133 patients, with a median progression-free interval (PFI) of 164 days. The integration of LASSO regression and Cox analysis resulted in a robust risk signature. The optimal lambda value was determined via tenfold cross-validation. Treatment factors such as the type of adjuvant therapy administered were explicitly included in the Cox analysis to evaluate their impact on patient outcomes. This adjustment for treatment heterogeneity ensures that the predictive accuracy of the nomogram is not confounded by differences in therapy, enhancing the clinical utility of the model in predicting patient outcomes.

LASSO regression with tenfold cross-validation yielded a prognostic model comprising ANK1, ARSI, CYGB, GLP1R, HSPA7, IGFBP6, NNAT, and PALM3 (Fig. 2A, B). The risk score formula, which combines Cox coefficients with categorical expression values, was established as follows: Risk score = (0.0735 * ANK1) + (0.04941 * ARSI) + (0.0163 * CYGB)–(0.0051 * GLP1R) + (0.0306 * HSPA7) + (0.06873 * IGFBP6) + (0.0218 * NNAT) + (0.0110 * PALM3).

Using a cut-off value of 1.790541, Kaplan–Meier analysis demonstrated significantly lower overall survival (OS) and progression-free interval (PFI) in high-risk patients compared to low-risk patients ($P < 0.001$). Functional validation of the model in the TCGA dataset confirmed its accuracy in predicting OS and PFI, with AUC values consistently exceeding 0.7. Predictive effectiveness over 1-, 2-, and 3-year periods was verified via ROC curve analysis for both OS and PFI (Fig. 2C–H).

3.3 Functional enrichment analysis of genes in high-risk and low-risk groups

Gene Set Enrichment Analysis (GSEA) was used to examine biological processes associated with genes in both high-risk and low-risk groups, highlighting the top three enriched pathways (Fig. 3). In the high-risk group, KEGG pathway analysis showed enhanced focal adhesion, chemokine signaling, and cytokine-cytokine receptor interactions. Reactome analysis

indicated enrichment in interleukin signaling, extracellular matrix organization, and neutrophil degranulation. Wikipathways analysis revealed enrichment in complete system, burn wound healing, and proinflammatory and profibrotic mediators.

Conversely, the low-risk group showed enrichment in pathways related to the cell cycle, spliceosome, and ribosome according to KEGG pathway analysis. Reactome analysis showcased enrichment in translation, processing of capped intron-containing pre-mRNA, and cell cycle mitotic pathways. GSEA analysis indicated a range of distinct biological activities in both high-risk and low-risk groups, providing insights into potential mechanisms contributing to differences in OS and PFI.

3.4 Screening and verification of prognosis-related DEGs

In our analysis of TCGA-READ DEGs, we identified key genes influencing GBM prognosis. Of the eight genes analyzed (ANK1, ARSI, CYGB, GLP1R, HSPA7, IGFBP6, NNAT, and PALM3), HSPA7 was excluded as it was identified as a pseudogene. The remaining seven genes underwent survival analysis. Using the median expression level of the 7-gene panel as a cutoff, patients were divided into high and low expression groups for survival analysis (Fig. 4).

Only three hub genes (NNAT, IGFBP6, and CYGB) showed significant correlations with poorer prognosis in Kaplan–Meier survival analysis ($P < 0.05$, Fig. 4). The other four genes did not exhibit significant differences in overall survival between high and low expression groups.

3.5 Prognostic significance of IDH status and three genes (NNAT, CYGB, IGFBP6) in glioblastoma

Table 2 presents the univariate and multivariate Cox regression analysis results for various prognostic factors, including IDH status, gender, race, age, Karnofsky Performance Score, and the three genes (NNAT, CYGB, IGFBP6). IDH status

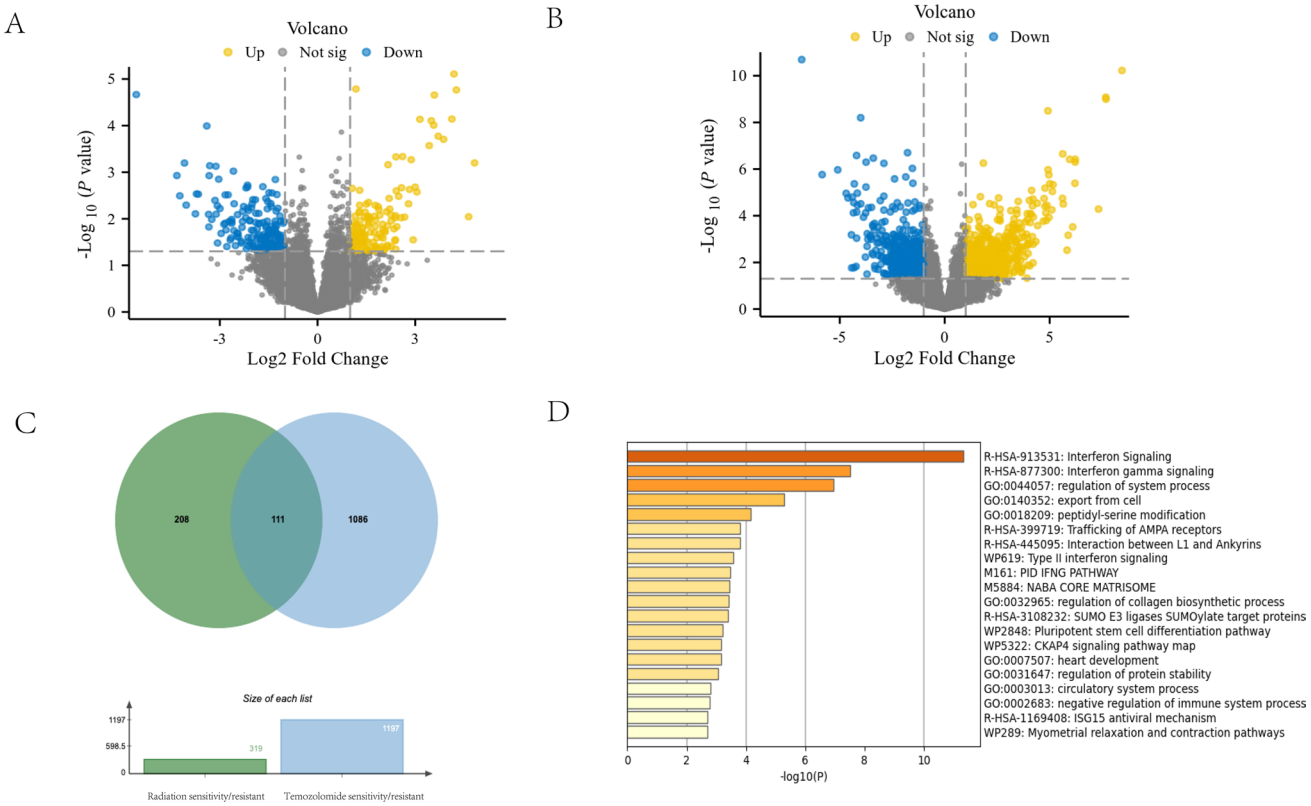

Fig. 1 Genetic profling and overall design to explore radiation/Temozolomide resistance. **A** Volcano plot of radiation resistant tissue vs. radiation sensitive tissue in GSE206225. |Log2 fold change|≥ 1 and P value ≤ 0.05 were set as cut-of values. **B** Volcano plot of Temozolomide resistanttissue vs. Temozolomide sensitive tissue in GSE206225. |Log2 fold change|≥ 1 and P value ≤ 0.05 were set as cut-of values. **C** The Venn diagram of diferentially expressed genes (DEGs) in radiation resistant/sensitive and Temozolomide resistant/sensitive. **D** 111 DEGs were imported into Metascape website for pathway enrichment analysis

demonstrated significant independent prognostic value in both univariate (HR = 0.301, P = 0.002) and multivariate analyses (HR = 0.389, P = 0.024), confirming its important role in glioblastoma prognosis. In the univariate analysis, NNAT and CYGB showed significant prognostic effects (NNAT: HR = 1.534, P = 0.016; CYGB: HR = 1.477, P = 0.029), and IGFBP6 was close to significance (HR = 1.368, P = 0.072). However, in the multivariate analysis, the significance of the three genes was reduced (NNAT: P = 0.090; CYGB: P = 0.364; IGFBP6: P = 0.286), suggesting that their prognostic effects may be influenced by IDH status and other factors.

3.6 Establishment and estimation of the three-gene prognostic signature

Three prognostic genes were assessed individually using Cox proportional hazards regression analysis to determine their significance for predicting GBM outcomes (Fig. 5). The risk score for the three genes was established using their respective Cox coefficients: risk score = (0.0819)*NNAT + (0.2281)*IGFBP6 + (0.1361)*CYGB.

As a result, individual risk scores for each patient were calculated and the median cut-off point was determined using R's "survminer" package, dividing patients into high-risk groups (n = 76) and low-risk groups (n = 77) (Fig. 5A). Figure 5B, C displays the survival outcomes of all patients in the training group along with a heatmap illustrating the three prognostic genes. The Kaplan–Meier survival curves indicate that the high-risk group had a poorer overall survival in comparison to the low-risk group (Fig. 5D). There was also a significant difference in the area under the curve (AUC) values in the three-gene prognostic signature for time-dependent ROC analysis (Fig. 5E) and for each gene individually (See Additional file 7: Fig. S1, S2, S3), indicating that the multi-gene model had superior predictive ability for 1-year, 2-year, and 3-year overall survival.

3.7 Expression analysis of hub genes in GBM

The expression analysis of NNAT, IGFBP6, and CYGB revealed significant downregulation in GBM samples compared to normal brain tissues (Fig. 6A). This consistent reduction suggests a potential role for these genes in tumor biology related to their loss or reduced function.

3.8 Study of the relationship between three hub genes and GBM-related genes

Genes associated with GBM tumorigenesis were obtained from the GeneCards database. The top 20 genes linked to GBM were analyzed, with significant expression differences noted between control and GBM groups (Fig. 6B). Pearson correlation analysis indicated associations between hub genes (NNAT, IGFBP6, CYGB) and GBM-related genes (Fig. 6C). For instance, high NNAT expression correlated positively with BRAF, HRAS, and MSH2, while high IGFBP6 expression correlated with ATM, BRAF, and CREBBP, and high CYGB correlated with EGFR, FBXW7, FGFR1, and MGMT.

3.9 An investigation of three hub genes' clinical predictive value using multiomics

We examined correlations between the three hub genes and immune-related genes from the TISIDB database, encompassing lymphocyte-related, chemokine-related, immunoinhibitor-related, MHC-related, immunostimulatory-related, and receptor-related categories (Fig. 7).

3.10 Analysis of the signaling pathways involved in NNAT, IGFBP6, and CYGB hub genes

In order to investigate how the hub genes impact specific signaling pathways, we examined their impact on the three signaling pathways. GSVA results revealed that high expression of NNAT primarily enriched in pathways such as kras_signaling_DN, estrogen_response_late, spermatogenesis, myogenesis, and pancreas beta cells, among others. Conversely, low expression of NNAT predominantly enriched in TGF_beta signaling, protein_secretion, and MYC targets v2. For IGFBP6, high expression was associated with enrichment in reactive_oxygen_species_pathway, inflammatory_response, apoptosis, epithelial_mesenchymal_transition, allograft_rejection, IL2_STAT5_signaling, and other pathways. On the contrary, low expression of IGFBP6 mainly enriched in MYC_targets_v2, mitotic_spindle, WNT_beta_catenin_signaling, E2F_targets, G2M_checkpoint, and other pathways. As for CYGB, high expression was linked to enrichment in pathways

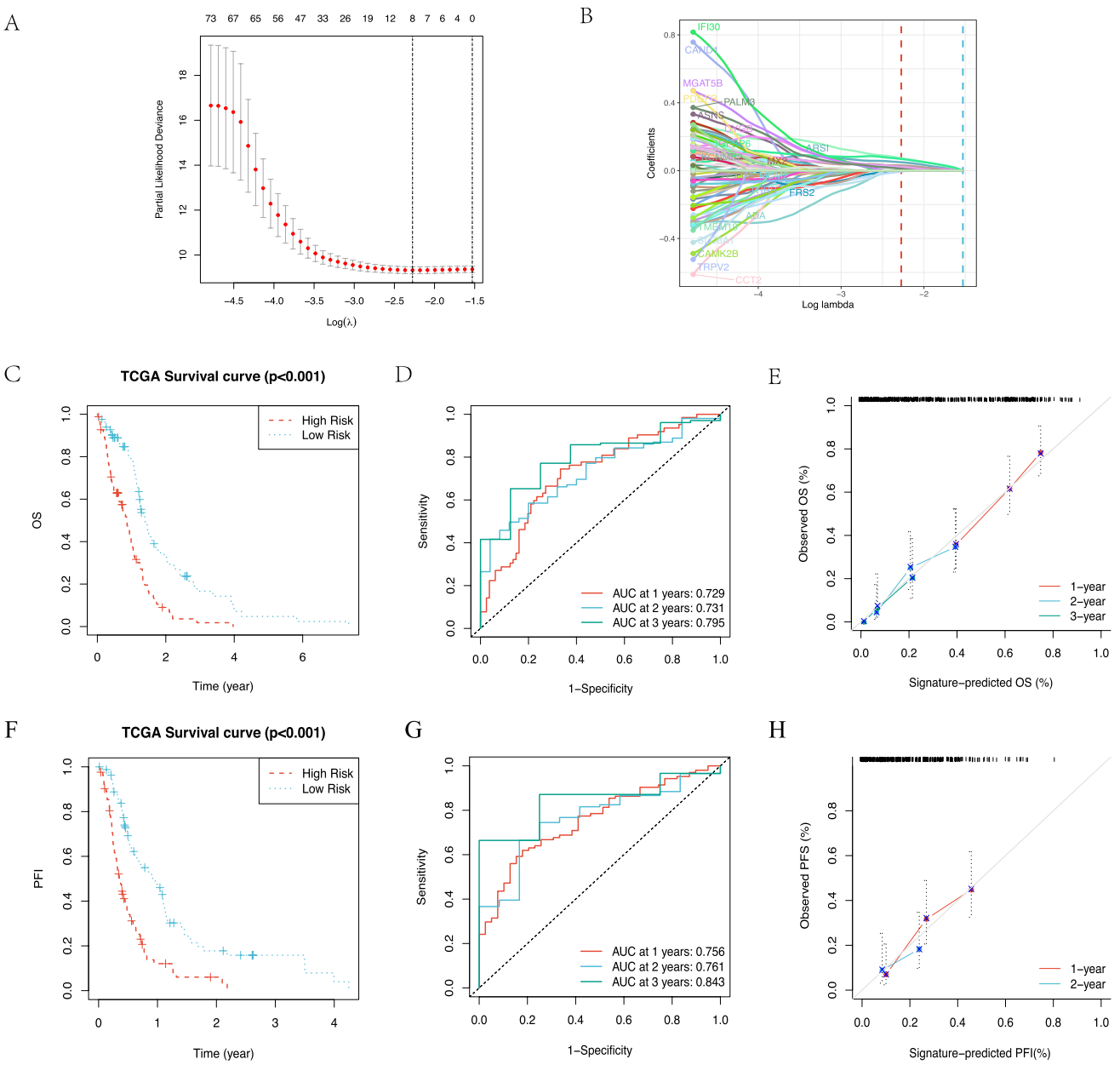

Fig. 2 Screening of variations using Lasso regression. **A** Depicts the variation characteristics of the coefficients of variables as identified through Lasso regression. **B** Illustrates the selection process for the optimal parameter value in the Lasso regression model, employing the cross-validation method. **C** Presents the survival curves of two groups based on overall survival (OS) and follow-up time. **D** Demonstrates the receiver operating characteristic (ROC) curve validating the prognostic efficiency over 1, 2, and 3 years. ROC—receiver operating characteristic; AUC—area under curve. **E** Displays the calibration curve for the overall survival nomogram model within the group. **F** Presents the survival curves of two groups based on Progression Free Interval (PFI) and follow-up time. **G** Demonstrates the ROC curve validating the prognostic efficiency of PFS over 1, 2, and 3 years. **H** Displays the calibration curve for the PFS nomogram model within the group

like reactive_oxygen_species_pathway, epithelial_mesenchymal_transition, IL6_JAK_STAT3_signaling, apical_junction, inflammatory_response, and myogenesis. In contrast, low expression of CYGB primarily enriched in mitotic_spindle, MYC_targets_v2, DNA_repair, E2F_targets, G2M_checkpoint, and other pathways (Fig. 8A–C).

These genes were also subjected to GSEA analysis, and Fig. 8D, E and F depicts the enriched pathways for these genes. Based on results, NNAT expression was high in pathways such as neuroactive ligand receptor interaction, calcium signaling pathway, and olfactory transduction, while NNAT expression was low in pathways such as allograft rejection,

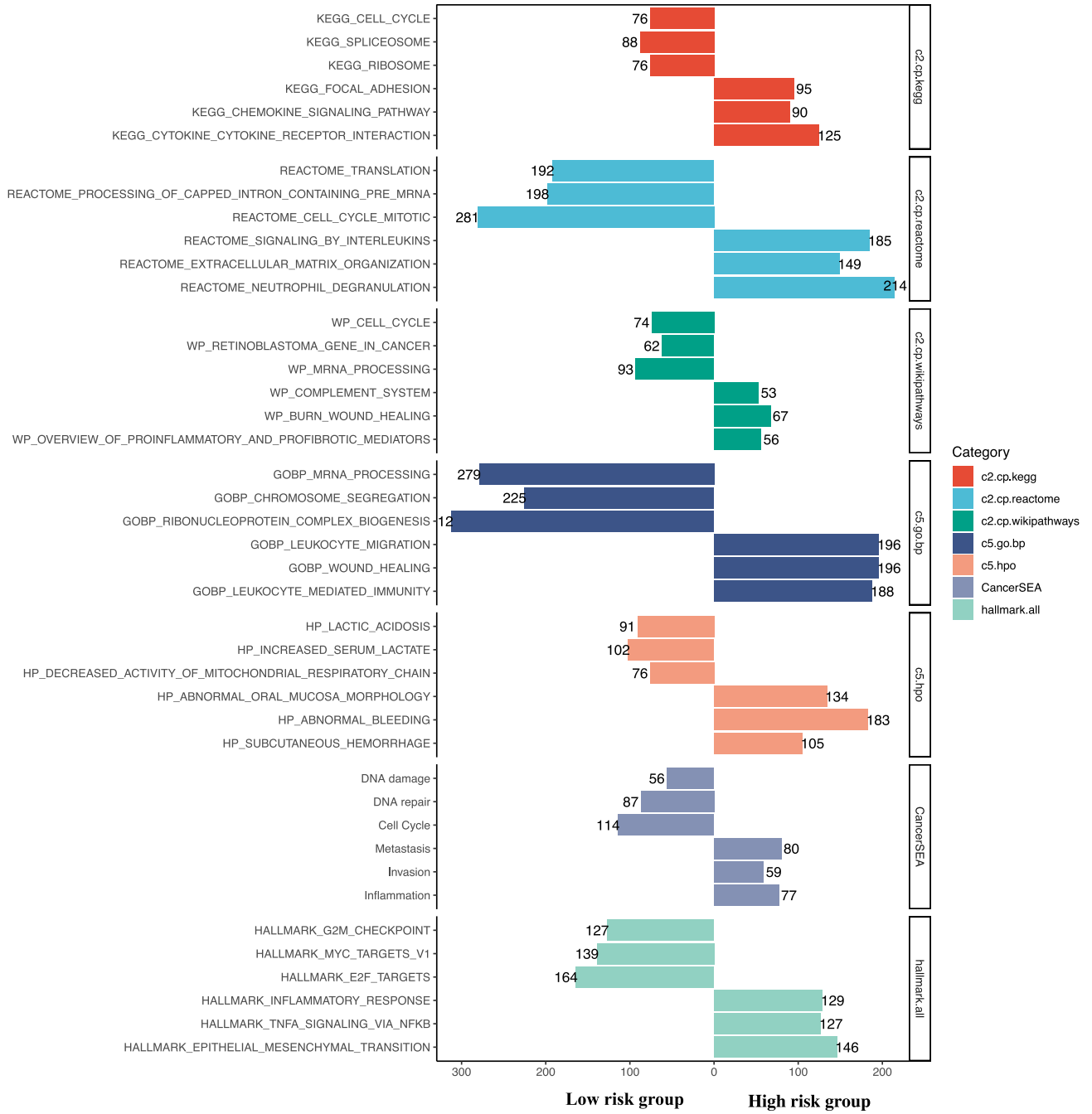

Fig. 3 The GSEA analysis of high-risk goup and low-risk goup expression which was grouped by the risk score model

autoimmune thyroid disease, and ribosome. Embryonic stem cells express high levels of IGFBP6 in signal pathway pathways involved in hematopoietic cell differentiation, complement cascades, and cytokine receptor interactions. high IGFBP6 expression occurs in notch signaling pathways, cell cycle pathways, and spliceosome pathways Conversely. Cytokine cytokine receptor interaction, chemokine signaling pathway, hematopoietic cell proliferation, and cytokine receptor interaction were associated with high expression of CYGB, whereas DNA replication, cell cycle, and spliceosome, were associated with low expression of CYGB.

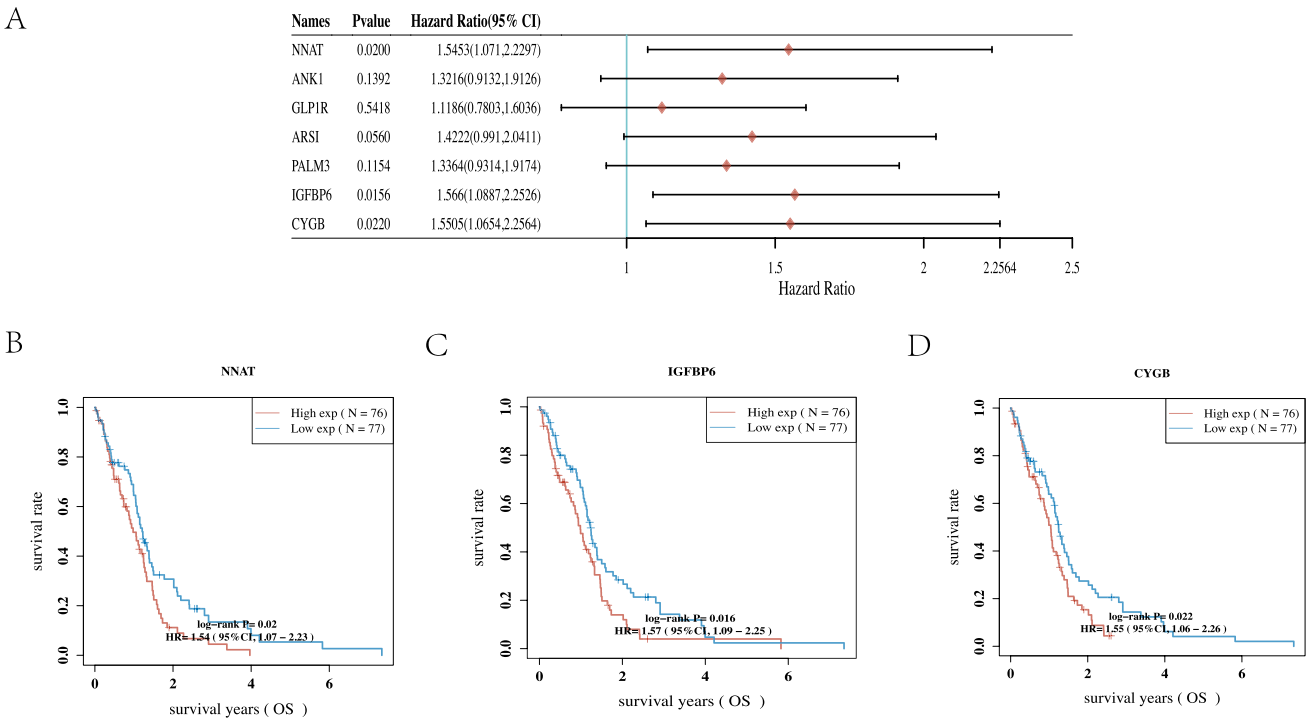

Fig. 4 Kaplan–Meier survival analysis of NNAT, ANK1, GLP1R, ARS1, PALM3, IGFBP6 and CYGB (**A**). Kaplan–Meier survival analysis of NNAT (**B**), IGFBP6 (**C**), CYGB (**D**). High expression of NNAT, IGFBP6 and CYGB were significantly associated with better overall survival compared to low expression by Kaplan–Meier survival analysis (P = 0.02, P = 0.016 and P = 0.022, respectively)

Table 2 Univariate and multivariate Cox regression analysis of prognostic factors in glioblastoma

Characteristics	Total (N)	Univariate analysis		Multivariate analysis	
		Hazard ratio (95% CI)	P value	Hazard ratio (95% CI)	P value
IDH status	161				
WT	149	Reference		Reference	
Mut	12	0.301 (0.138–0.654)	**0.002**	0.389 (0.171–0.883)	**0.024**
Age	168				
< = 60	87	Reference		Reference	
> 60	81	1.365 (0.973–1.915)	0.072	1.123 (0.783–1.611)	0.529
Karnofsky performance score	128				
< 80	36	Reference			
> 80	92	0.838 (0.538–1.305)	0.434		
Gender	168				
Female	59	Reference			
Male	109	1.026 (0.719–1.466)	0.887		
NNAT	168				
Low	84	Reference		Reference	
High	84	1.534 (1.083–2.174)	**0.016**	1.363 (0.953–1.950)	0.090
IGFBP6	168				
Low	84	Reference		Reference	
High	84	1.368 (0.973–1.923)	0.072	1.229 (0.841–1.796)	0.286
CYGB	168				
Low	84	Reference		Reference	
High	84	1.477 (1.041–2.096)	**0.029**	1.198 (0.811–1.767)	0.364

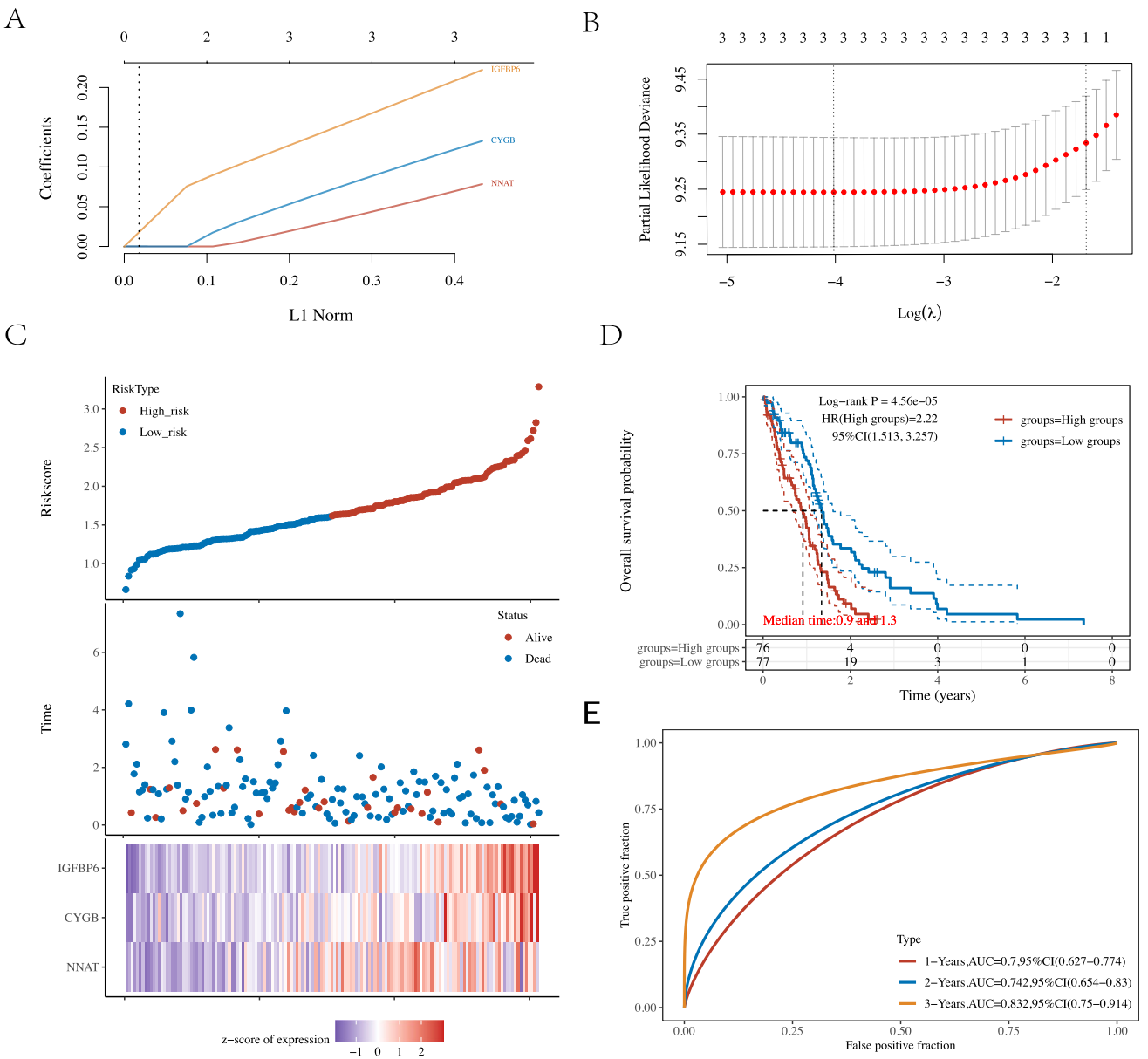

Fig. 5 Risk model for GBM patients based on the hub genes. **A** The tuning parameters (log λ) of OS-related proteins were selected to cross-verify the error curve. According to the minimal criterion and 1-se criterion, perpendicular imaginary lines were drawn at the optimal value. **B** The LASSO coefficient profile of genes and perpendicular imaginary line were drawn at the value chosen by tenfold cross-validation. **C** Risk score, survival time and survival status, expression of 3 hub genes in the training cohort; **D** KM survival curve distribution of 3 hub genes(IGFBP6, CYGB, NNAT) signature in the training cohort; **E** ROC curve and AUC of 3 hub genes signature classification

3.11 PPI network construction and analysis

A protein-interaction network was constructed using STRING (Fig. 9). Functional enrichments associated with NNAT, IGFBP6, and CYGB were observed in molecular functions such as growth factor binding and hormone activity. Enrichment was also noted in pathways like aldosterone-regulated sodium reabsorption and ovarian steroidogenesis (Table 3). This analysis provides insights into the functional relationships of hub genes and their involvement in GBM pathogenesis.

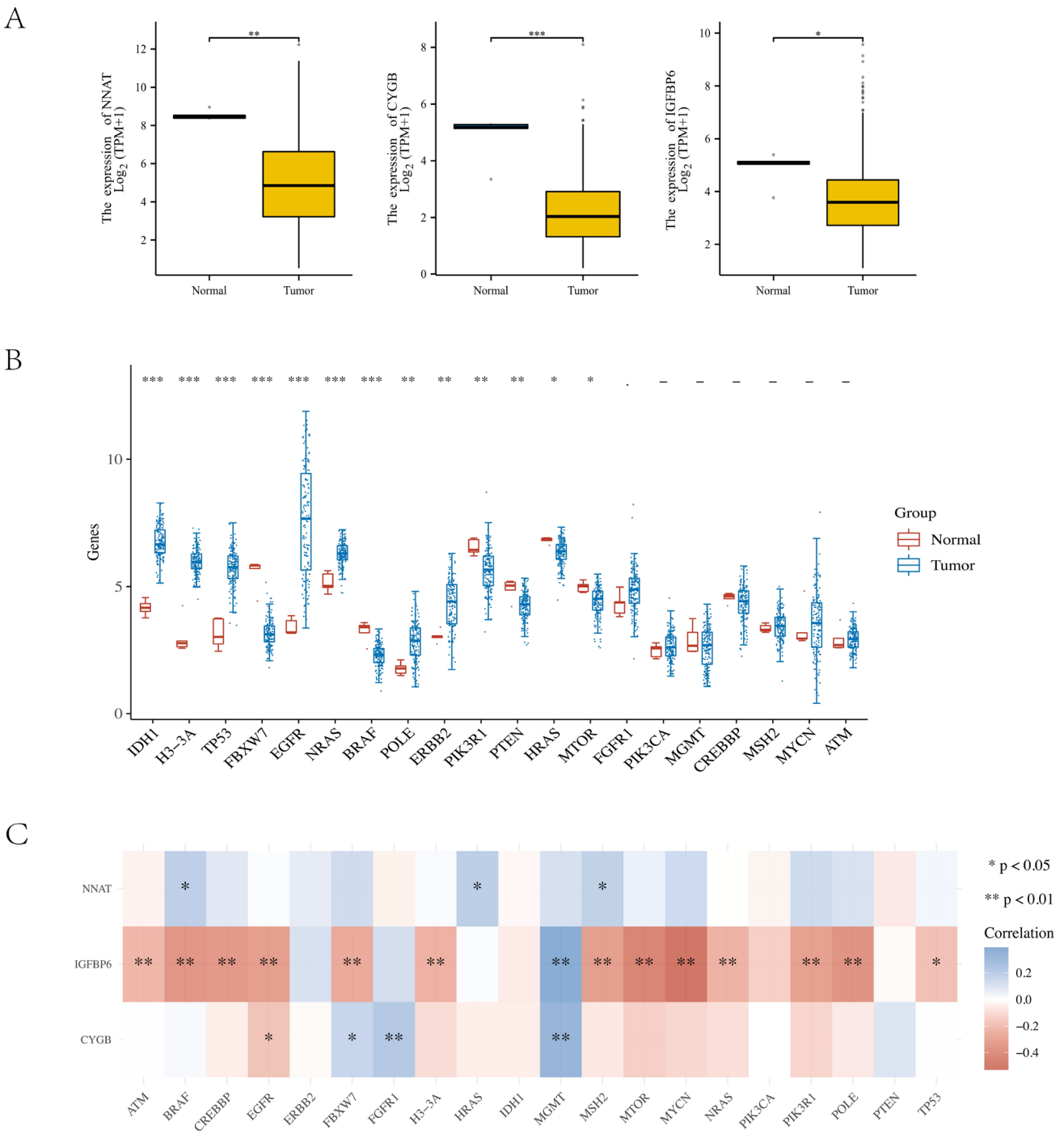

Fig. 6 The relationship of hub genes and the GBM-related genes. **A** The comparisons of the expression of the 3 hub genes between the normal and GBM patients. **B** The comparisons of the expression of multiple GBM-related genes between the normal and GBM patients. **C** The Pearson correlations between three hub genes (NNAT, IGFBP6 and CYGB) and GBM-related genes (* represented $P < 0.05$, ** represented $P < 0.01$)

3.12 Nomogram construction and calibration curves for predicting GBM outcome

Using TCGA's GBM dataset, we developed a nomogram incorporating NNAT, IGFBP6, CYGB, and clinical parameters such as age, gender, IDH status, and Karnofsky Performance Scores (Fig. 10A). Calibration curves indicated good alignment

between predicted and observed overall survival at one, two, and three years, supporting the clinical applicability of the nomogram (Fig. 10B).

3.13 Clinical validation results of NNAT, IGFBP6, and CYGB expression levels

Validation results from multiple datasets consistently showed poorer prognosis in the high-expression group (Fig. 11). IHC data from the Human Protein Atlas depicted differential expression of IGFBP6 in GBM and normal tissues, while no significant expression of CYGB was noted in either tissue type (Fig. 12). These variations suggest that the distinct expression levels of these hub genes may relate to inherent biological differences among GBM patients.

4 Discussion

The standard post-surgical treatment regimen of Glioblastoma (GBM) is temozolomide (75 mg/m^2) and radiation for 6 weeks, followed by adjuvant temozolomide (150–200 mg/m^2) every 28 days for six cycles [16]. The most widely used chemical therapy for GBM is temozolomide, a small molecular alkylating agent that methylates DNA purine bases directly [24]. O^6-methylguanine lesions are responsible for the primary cytotoxic action, which induces apoptosis, autophagy, and cellular senescence [25–28]. Further, when administered concurrently with radiation therapy, temozolomide appears to have radiation-sensitizing properties, increasing the likelihood that radiation-induced DNA double-strand breaks will occur and that cells will die [29].

Chemoresistance is common in numerous cases of GBM, either due to inherent factors or acquired traits. An essential resistance mechanism to temozolomide treatment in GBM involves the methylation of the Methyl guanine methyl transferase (MGMT) gene promoter, leading to gene silencing and downregulation. MGMT, functioning as a repair gene, plays a crucial role by eliminating alkyl groups from the O^6 position of guanine, thereby mitigating the impact of temozolomide and other alkylating drugs [30]. Hence, focusing on transcriptional factors or epigenetic alterations associated with MGMT activation could be considered as potential options in GBM therapy [18].

Radiation therapy (RT), a cornerstone of traditional cancer treatment for GBM, demonstrates significant efficacy in eliminating or controlling specific tumors when used in conjunction with surgery and other therapies. However, the response of individual cells to radiation can vary, leading to disparate treatment outcomes. Resistance to radiation therapy is influenced by numerous factors, including mechanisms for repairing radiation-induced DNA damage, cell cycle arrest, evasion of apoptosis, the abundance of cancer stem cells, alterations in cancer cells and their microenvironment, the presence of exosomal and non-coding RNAs, metabolic reprogramming, and the occurrence of ferroptosis [31].

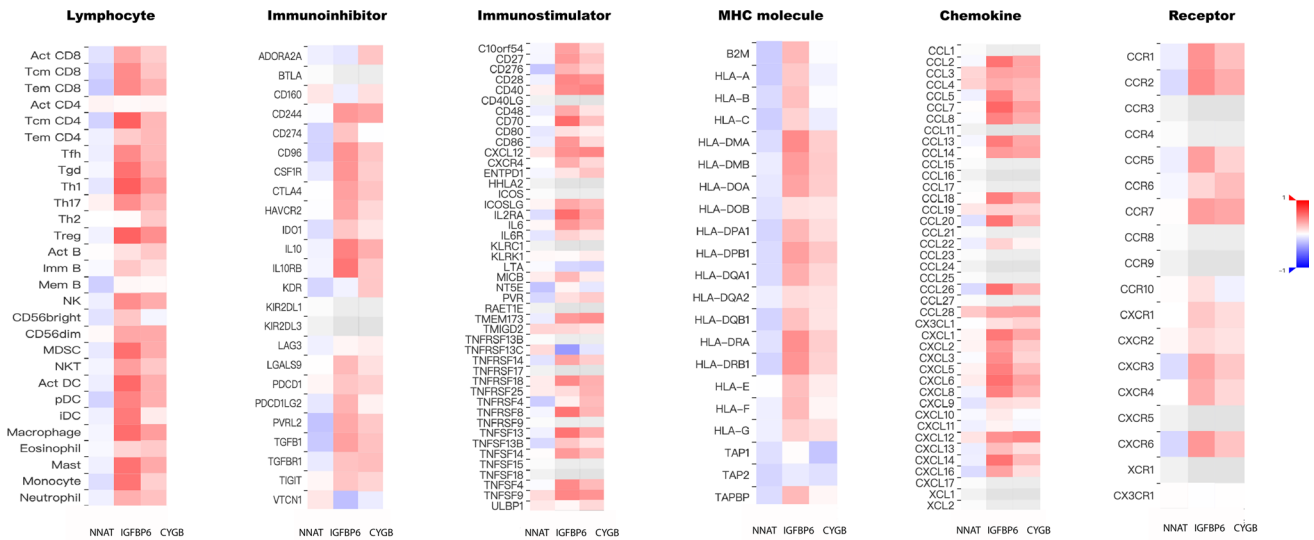

Fig. 7 Spearman correlations between expression of NNAT, IGFBP6 and CYGB (X axis) and lymphocyte, Immunoinhibitor, Immunostimulator, MHC molecule, Chemokine and receptor (Y axis) across GBM

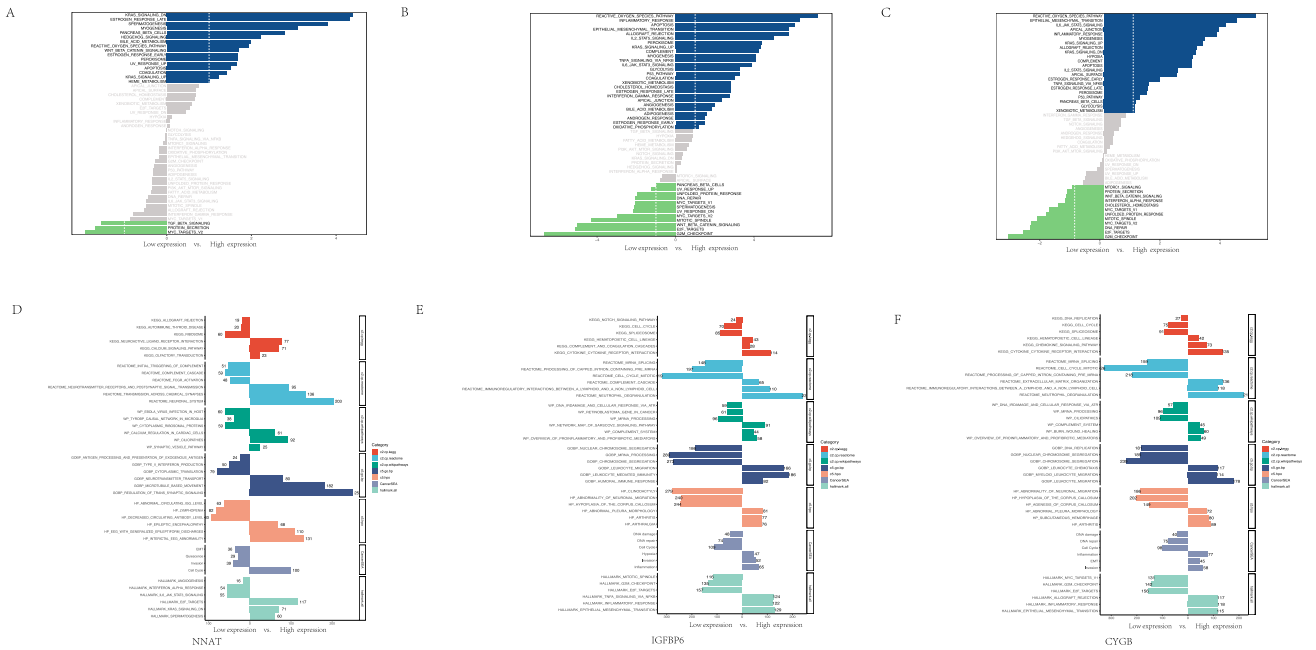

Fig. 8 GSVA and GSEA analysis of high and low expression of NNAT, IGFBP6 and CYGB. **A** GSVA of NNAT; **B** GSVA of IGFBP6; **C** GSVA of CYGB; **D** GSEA of NNAT; **E** GSEA of IGFBP6; **F** GSEA of CYGB

Despite the study of therapeutic resistance and hundreds of ongoing clinical trials, The therapeutic effect of GBM has not improved since 2005 [16]. Understanding the complex biology of GBM, particularly the mechanisms underlying radiotherapy sensitivity, is crucial for developing effective treatments. Comprehensive research on the regulatory networks of long non-coding RNAs (lncRNAs) related to therapy resistance is still lacking, particularly based on clinical specimens.

To address these gaps, we conducted systematic bioinformatics analyses to identify potential biomarkers and mechanisms linked to radiotherapy resistance in GBM patients. Using the GEO dataset GSE206225, we identified 319 and 1197

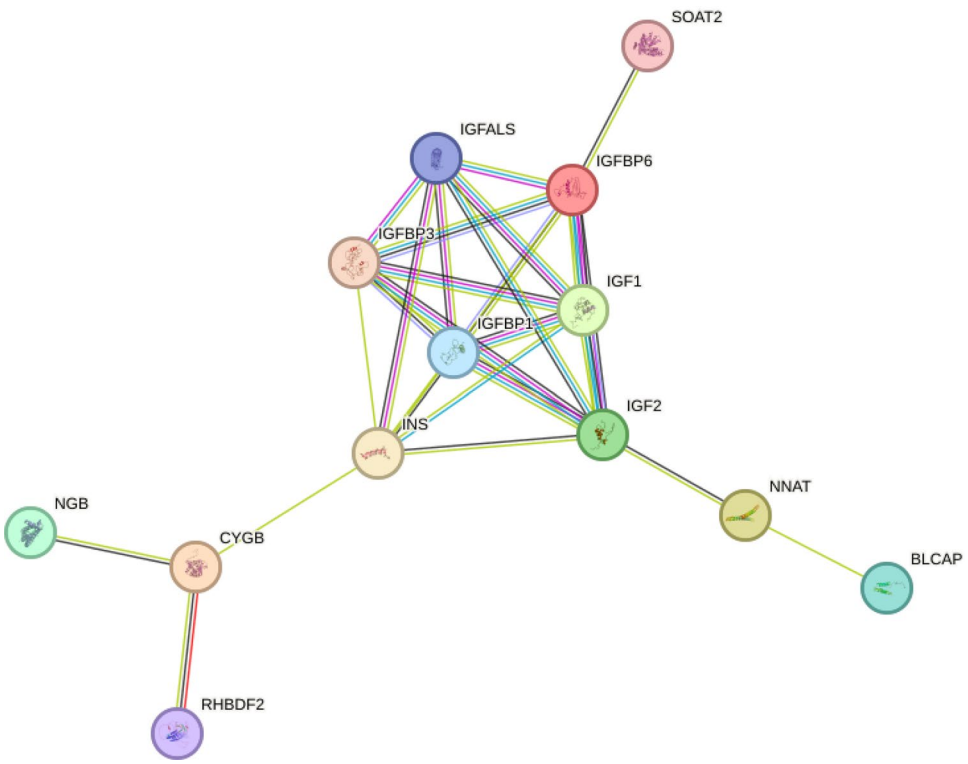

Fig. 9 PPI network of 3 hub genes was constructed in STRING

differentially expressed genes (DEGs) between radiation-sensitive vs. resistant groups and temozolomide-sensitive vs. resistant groups, respectively. We focused on the intersection of these DEGs to uncover shared mechanisms influencing treatment response, identifying 111 common DEGs. This intersectional approach enabled us to conduct a comprehensive evaluation of tumor responses to both radiation and temozolomide, identifying shared genetic markers for targeted interventions. Metascape enrichment analysis revealed that these DEGs were predominantly enriched in pathways related to interferon signaling, system regulation, and cellular export, suggesting involvement of immune and regulatory processes in treatment response.

To develop a predictive model for GBM prognosis, we used LASSO regression and identified eight key genes (ANK1, ARSI, CYGB, GLP1R, HSPA7, IGFBP6, NNAT, PALM3) that formed the basis for calculating a risk score. This model effectively stratified patients into high- and low-risk groups, demonstrating significant differences in overall survival (OS) and progression-free interval (PFI). The model's predictive power was validated through ROC curve analysis. Further analysis identified three hub genes—NNAT, IGFBP6, and CYGB—that were significantly associated with patient survival. A nomogram was then constructed, integrating these hub genes with key clinical parameters (age, sex, IDH mutation status, and Karnofsky Performance Score). This comprehensive approach improved risk stratification by combining genetic and clinical factors, thereby enhancing the accuracy of OS and PFI predictions.

In this study, we employed both standard Cox regression and Lasso-Cox regression to construct and refine the prognostic model. Standard Cox regression was used for univariate and multivariate analysis to assess the independent prognostic impact of each variable on overall survival (OS). However, due to potential multicollinearity among variables, we also used Lasso-Cox regression. Lasso-Cox, with its regularization technique, automatically selects the most predictive variables by reducing multicollinearity, thus yielding a more robust model. Combining these two approaches allowed us to comprehensively evaluate prognostic factors while enhancing model stability and predictive accuracy. Our multivariate Cox regression analysis indicates that although NNAT, IGFBP6, and CYGB show prognostic value in univariate analysis, their independence may be moderated by IDH status and other clinical factors. This highlights the importance of considering IDH status and other clinical characteristics when interpreting the prognostic value of these three genes in clinical applications. Lasso-Cox regression with Survival analysis confirmed that elevated expression levels of NNAT, IGFBP6, and CYGB correlated with poorer prognosis, forming a robust three-gene prognostic signature with enhanced predictive efficacy for 1-year, 2-year, and 3-year OS.

Neuronatin (NNAT), identified in 1994, has garnered attention for its distinctive expression in the neonatal mammalian brain [32, 33]. NNAT plays diverse roles in tissue and organ development, as well as in adult organisms [33, 34], its involvement in the differentiation of keratinocytes and adipose tissue cells has been suggested [35, 36]. NNAT exhibits various physiological functions, including influencing insulin secretion [37], synaptic plasticity [38], calcium-induced cell migration [39], stress response [40] and etc. [41, 42]. Reports have linked NNAT protein levels with tissue degeneration, cancer, clinical diagnosis, and the etiological factors of various diseases [43, 44]. Downstream signaling studies have explored its impact on intracellular Ca^{2+} levels, regulation of Ca^{2+} ATPase in the endoplasmic reticulum (ER), and reduction in glucose-mediated insulin secretion, among others [45–47]. There has been considerable attention paid recently to NNAT's relationship with cancer [48].A cytosine methylation signal can be modulated by NNAT's three CpG islands in its promoter region [49]. Embryonic neoplasms such as Wilm's tumor are characterized by aberrant cell growth when methylation is lost in this imprint control region [50]. Methylation loss and subsequent alterations in NNAT expression impact the growth phase of medulloblastoma [43, 51], neuroblastoma [52, 53], osteosarcoma [54], hepatocellular carcinoma [55] and myxoid liposarcoma [56]. NNAT is also related to lung cancer [57, 58], breast cancer [59], pediatric leukemia [60] and other kinds of cancer. A study investigating factors contributing to chemotherapy resistance and GBM tumor recurrence identified NNAT as one of the differentially expressed proteins in tumor stem cells. Elevated NNAT expression was found in a distinct subset of primary GBM tumors and was significantly correlated with increased cellular proliferation and reduced patient survival [61].

Insulin-like growth factor binding protein 6 (IGFBP6), a gene encoding a protein, possesses various insulin-like growth factor (IGF)-independent actions, including inducing tumor cell migration, and modulating cell survival and differentiation [62]. IGFBP6 have been confirmed to be related to many cancer, such as neuroblastoma [63], colorectal cancer [64], ovarian cancer [65], nasopharynx cancer [66], esophagus cancer [67] and other cancers. Some studies suggested that IGFBP6 might be an important regulator and prognostic factor for glioma and a potential therapeutic target for glioma patients [68, 69]. Several studies have indicated that IGFBP6 plays a role in immune infiltration and contributes to remodeling the tumor microenvironment in GBM [70, 71]. IGFBP6 was identified as a molecular subtype and an oxidative stress-related prognostic biomarker in GBM through integrated analysis of multiomics data [72]. Researchers also

Table 3 Functional enrichments in the network of 3 hub genes

Term	Description	Background gene count	Background gene count	p-value
Molecular function (Gene Ontology)				
GO:0005520	Insulin-like growth factor binding	4 of 17	2.55	3.34e−06
GO:0019838	Growth factor binding	5 of 127	1.78	3.79e−05
GO:0031995	Insulin-like growth factor II binding	3 of 8	2.75	6.06e−05
GO:0031994	Insulin-like growth factor I binding	3 of 10	2.66	7.87e−05
GO:0005159	Insulin-like growth factor receptor binding	3 of 16	2.45	0.00021
GO:0005158	Insulin receptor binding	3 of 23	2.3	0.00047
GO:0005344	Oxygen carrier activity	2 of 15	2.31	0.0383
GO:0005179	Hormone activity	3 of 129	1.55	0.0493
Cellular component (Gene Ontology)				
GO:0016942	Insulin-like growth factor binding protein complex	4 of 5	3.08	2.93e−08
GO:0042567	Insulin-like growth factor ternary complex	3 of 4	3.06	5.34e−06
Local network cluster (STRING)				
CL:24,268	Insulin-like growth factor-binding protein family 1–6, chordata, and Insulin-like growth factor	6 of 10	2.96	7.70e−13
CL:24,270	Insulin-like growth factor, and Insulin-like growth factor-binding protein family 1–6, chordata	3 of 5	2.96	1.43e−05
CL:31,175	Mixed, incl. intracellular oxygen transport, and plus-end directed microfilament motor activity	2 of 6	2.7	0.0103
CL:27,934	Mostly uncharacterized, incl. MCT-1/Tma20, and Sarcoglycan alpha/epsilon	2 of 11	2.44	0.0238
KEGG pathway				
hsa04960	Aldosterone-regulated sodium reabsorption	2 of 37	1.91	0.0493
hsa04913	Ovarian steroidogenesis	2 of 50	1.78	0.0493
hsa04935	Growth hormone synthesis, secretion and action	3 of 117	1.59	0.0202
hsa04014	Ras signaling pathway	3 of 225	1.31	0.0493
Reactome pathways				
HSA-8981607	Intracellular oxygen transport	2 of 3	3.0	0.0046
HSA-2428933	SHC-related events triggered by IGF1R	2 of 9	2.53	0.0167
HSA-422085	Synthesis, secretion, and deacylation of Ghrelin	2 of 18	2.23	0.0432
HSA-381426	Regulation of Insulin-like Growth Factor (IGF) transport and uptake by Insulin-like Growth Factor Binding Proteins (IGFBPs)	6 of 124	1.87	2.76e−07
HSA-392499	Metabolism of proteins	7 of 1917	0.74	0.0432
WikiPathways				
WP2406	Cardiac progenitor differentiation	3 of 53	1.93	0.0048
Disease-gene associations (DISEASES)				
DOID:9521	Laron syndrome	2 of 3	3.0	0.0184
DOID:2018	Hyperinsulinism	2 of 9	2.53	0.0337
DOID:26	Pancreas disease	3 of 70	1.81	0.0312

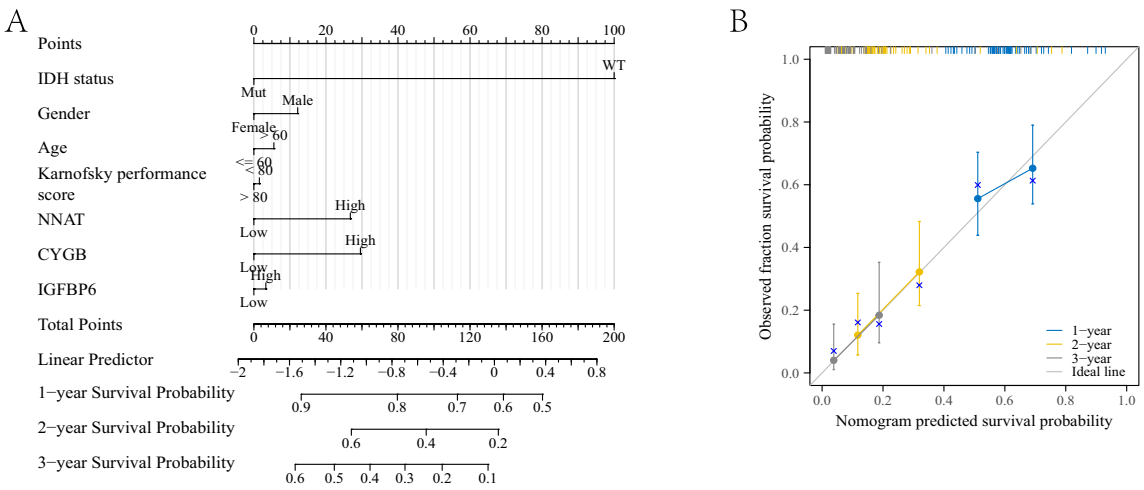

Fig. 10 Nomogram for prediction of the outcome of patients with GBM. **A** For the OS, Nomogram was constructed based on the expression of NNAT, IGFBP6 and CYGB and the clinical parameters. **B** Calibration curves of nomogram for predicting OS at 1-year, 2-year and 3-year in the TCGA GBM dataset

revealed that IGFBP6 secreted from temozolomide-sensitive cells influences the paracrine mechanism, impacting tumor proliferation and survival in chemoresistant cells [73].

Cytoglobin (CYGB) is approximately 25% similar to vertebrate myoglobin and hemoglobin, and 16% similar to human neuroglobin. CYGB has been found in neurons, solitary tracts, hepatocytes, and progenitor cells [74]. CYGB is dynamically responsive to insults like fibrosis, oxidative stress, and hypoxia, and it has been implicated in cancer [75], Its downregulation in most cancer cells due to hypermethylation suggests it may function as a tumor suppressor gene [76, 77]. Conversely, in some malignancies, CYGB is upregulated, potentially linked to resistance to hypoxia [78]. Studies have shown that human GBM cell lines express CYGB, with significant increases in expression under hypoxic conditions, suggesting it may contribute to defense mechanisms that enable cancer cells to survive in hypoxic environments [79–81].

Based on previous research on NNAT, IGFBP6, and CYGB, and our current findings, we believe that these three hub genes play a crucial role in radiotherapy and chemotherapy resistance in GBM.

Pearson correlation analysis indicated significant associations between NNAT, IGFBP6, CYGB, and various GBM-related genes. Elevated NNAT expression was positively correlated with BRAF, HRAS, and MSH2; increased IGFBP6 expression was associated with higher levels of ATM, BRAF, and CREBBP; CYGB was positively correlated with EGFR, FBXW7, FGFR1, and MGMT. This provides insights into potential molecular mechanisms underlying GBM development and progression.

Further analyses examined relationships between these hub genes and immune-related genes, emphasizing their potential roles in modulating immune responses in GBM. Correlations between NNAT, IGFBP6, and CYGB with various immune-related gene categories revealed their intricate involvement in the tumor microenvironment. Our findings are consistent with previous studies showing that IGFBP6 and CYGB, especially IGFBP6, play crucial roles in immune responses [82–84].

GSVA and GSEA analyses uncovered the functional roles of these genes, including their involvement in signaling pathways related to growth, inflammation, apoptosis, and cell cycle regulation. Protein–protein interaction network construction provided a comprehensive view of the functional enrichments associated with the three hub genes, highlighting their potential biological roles in GBM.

The integration of clinical characteristics and the hub genes into a nomogram demonstrated its clinical utility, supported by good agreement between predicted and observed survival probabilities. By combining clinical parameters and novel molecular markers, this nomogram enables clinicians to differentiate high-risk patients who may benefit from more aggressive treatment from those with better prognosis, thus guiding personalized treatment decisions.

This study has several important limitations that should be acknowledged. This study has several limitations. Firstly, the analysis was conducted using the GEO dataset GSE206225 and TCGA database, which may limit the generalizability of our findings due to the specific characteristics and sample sizes of these datasets. The absence of patient-derived xenograft (PDX) models limits the translational relevance of our findings, as PDX models are essential for evaluating tumor heterogeneity and confirming the efficacy of proposed biomarkers in a clinical-like setting. Additionally, our data did not include comprehensive molecular classification information, such as IDH mutation status or 1p/19q co-deletion,

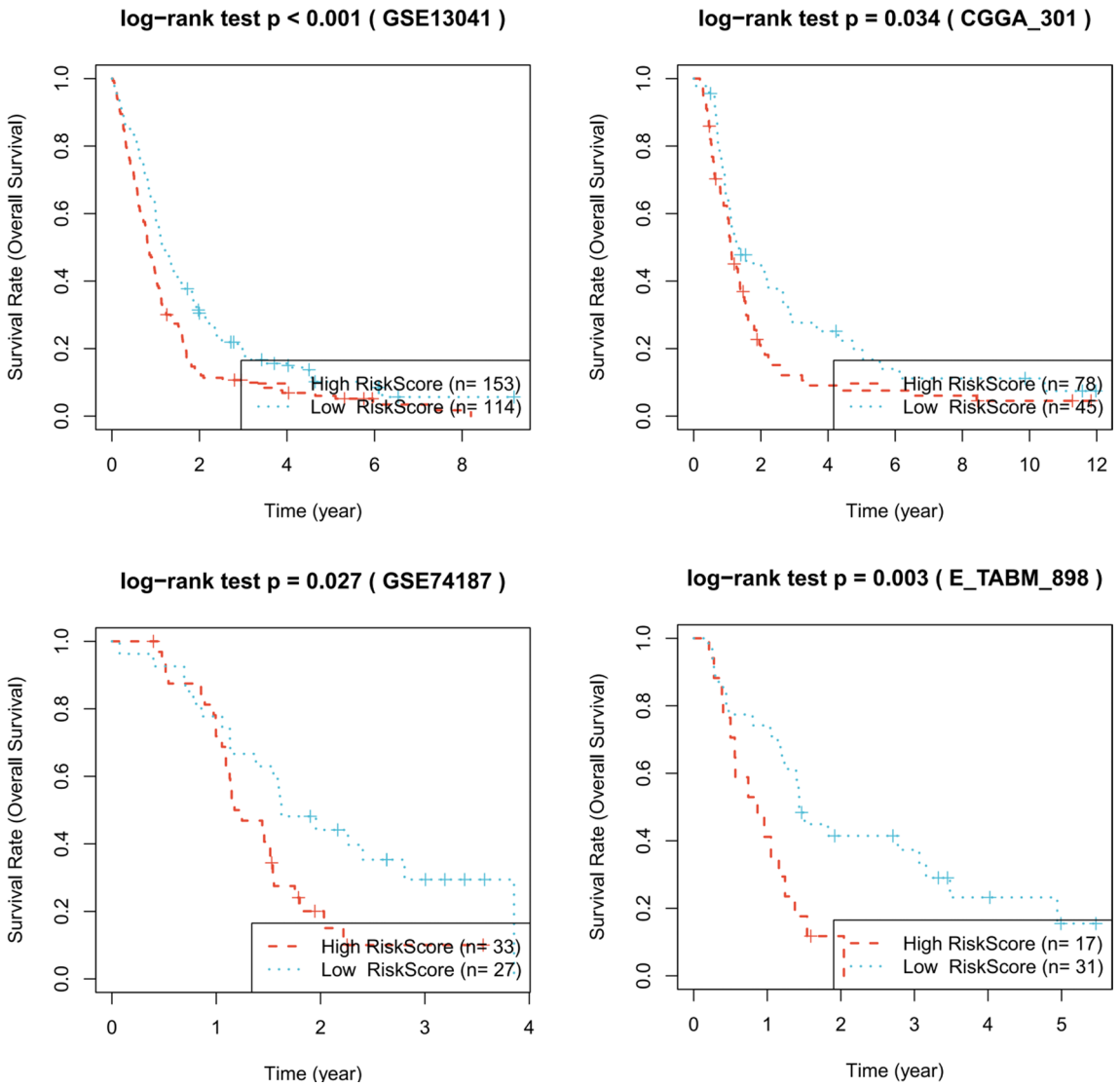

Fig. 11 Validation of the three-gene (NNAT, IGFBP6 and CYGB) risk signature through multiple external cohorts

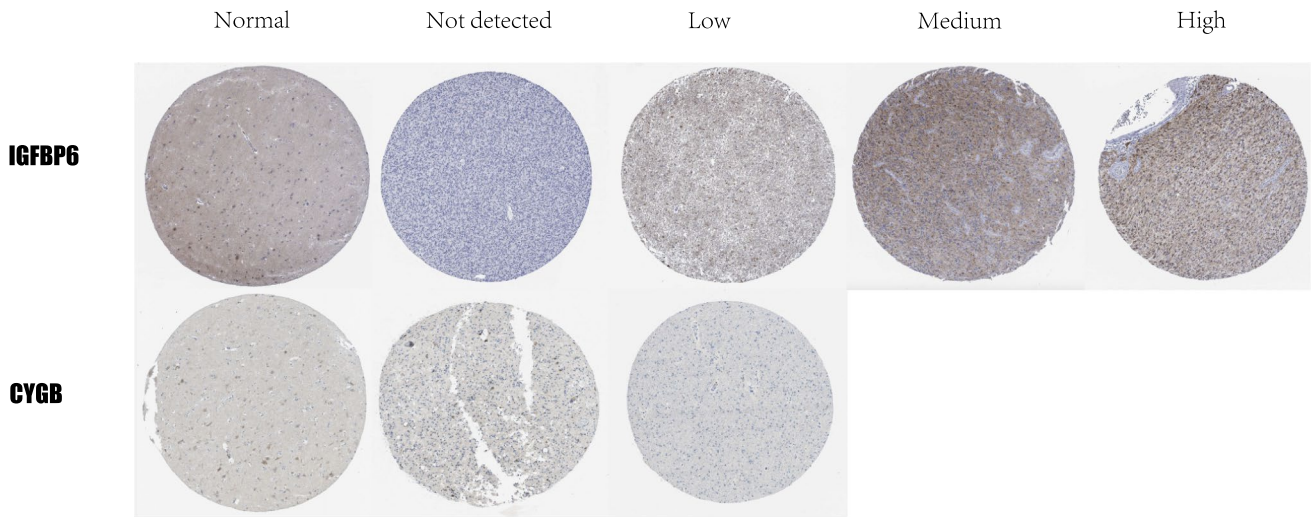

Fig. 12 The protein expression levels of NNAT, IGFBP6 and CYGB in brain tissues and GBM tissue from HPA online database

per the 2021 WHO classification of CNS tumors. The retrospective nature of our data and potential confounding factors may also impact the reliability of these results.

While our diagnostic and prognostic models showed promising performance, the absence of experimental validation limits our conclusions regarding the functional roles of these genes in GBM development and treatment response. Future research incorporating updated molecular classifications, PDX models, and prospective validation in larger, diverse populations will be crucial to verify the clinical utility of our model and biomarkers.

In conclusion, our study sheds light on the mechanisms of GBM treatment resistance, particularly in the context of radiotherapy and temozolomide sensitivity. The identified three-gene signature (NNAT, IGFBP6, CYGB) holds promise for enhancing prognostic accuracy and guiding future research and therapeutic interventions for patients with GBM. However, further experimental validation and evaluation in diverse populations are warranted to establish the clinical utility of these findings.

Acknowledgements Not applicable.

Author contributions Jing Zhu and Jinmin Xue designed the study. Jing Zhu and Jie Zhang coordinated the study and the data acquisition. Jie Zhang and Jinmin Xue performed the statistical analyses and interpreted the results. Jing Zhu and Jinmin Xue drafted the manuscript. All authors read and approved the final manuscript.

Funding This study have no funding.

Data Availability The datasets analyzed for this study can be found in the TCGA-COAD/READ project (http://www.cancer.gov/tcga) and GEO (https://www.ncbi.nlm.nih.gov/geo/).

Declarations

Ethics approval and consent to participate This article does not contain any studies with human participants or animals performed by any of the authors.

Competing interests The authors declare no competing interests.

Open Access This article is licensed under a Creative Commons Attribution-NonCommercial-NoDerivatives 4.0 International License, which permits any non-commercial use, sharing, distribution and reproduction in any medium or format, as long as you give appropriate credit to the original author(s) and the source, provide a link to the Creative Commons licence, and indicate if you modified the licensed material. You do not have permission under this licence to share adapted material derived from this article or parts of it. The images or other third party material in this article are included in the article's Creative Commons licence, unless indicated otherwise in a credit line to the material. If material is not included in the article's Creative Commons licence and your intended use is not permitted by statutory regulation or exceeds the permitted use, you will need to obtain permission directly from the copyright holder. To view a copy of this licence, visit http://creativecommons.org/licenses/by-nc-nd/4.0/.

References

1. Wirsching HG, Galanis E, Weller M. Glioblastoma. Handb Clin Neurol. 2016;134:381–97. https://doi.org/10.1016/b978-0-12-802997-8.00023-2.
2. Dolecek TA, Propp JM, Stroup NE, Kruchko C. CBTRUS statistical report: primary brain and central nervous system tumors diagnosed in the United States in 2005–2009. Neuro Oncol. 2012;14(Suppl 5):v1-49. https://doi.org/10.1093/neuonc/nos218.
3. Porter KR, McCarthy BJ, Freels S, Kim Y, Davis FG. Prevalence estimates for primary brain tumors in the United States by age, gender, behavior, and histology. Neuro Oncol. 2010;12:520–7. https://doi.org/10.1093/neuonc/nop066.
4. Farrell CJ, Plotkin SR. Genetic causes of brain tumors: neurofibromatosis, tuberous sclerosis, von Hippel-Lindau, and other syndromes. Neurol Clin. 2007;25:925–46, viii. https://doi.org/10.1016/j.ncl.2007.07.008.
5. Goodenberger ML, Jenkins RB. Genetics of adult glioma. Cancer Genet. 2012;205:613–21. https://doi.org/10.1016/j.cancergen.2012.10.009.
6. Fisher JL, Schwartzbaum JA, Wrensch M, Wiemels JL. Epidemiology of brain tumors. Neurol Clin. 2007;25(867–890):vii. https://doi.org/10.1016/j.ncl.2007.07.002.
7. Ron E, et al. Tumors of the brain and nervous system after radiotherapy in childhood. N Engl J Med. 1988;319:1033–9. https://doi.org/10.1056/nejm198810203191601.
8. Barchana M, Margaliot M, Liphshitz I. Changes in brain glioma incidence and laterality correlates with use of mobile phones—a nationwide population based study in Israel. Asian Pac J Cancer Prev. 2012;13:5857–63. https://doi.org/10.7314/apjcp.2012.13.11.5857.
9. Joseph GP, McDermott R, Baryshnikova MA, Cobbs CS, Ulasov IV. Cytomegalovirus as an oncomodulatory agent in the progression of glioma. Cancer Lett. 2017;384:79–85. https://doi.org/10.1016/j.canlet.2016.10.022.

10. Deltour I, et al. Mobile phone use and incidence of glioma in the Nordic countries 1979–2008: consistency check. Epidemiology. 2012;23:301–7. https://doi.org/10.1097/EDE.0b013e3182448295.
11. Little MP, et al. Systematic review and meta-analysis of circulatory disease from exposure to low-level ionizing radiation and estimates of potential population mortality risks. Environ Health Perspect. 2012;120:1503–11. https://doi.org/10.1289/ehp.1204982.
12. Rice T, et al. Understanding inherited genetic risk of adult glioma—a review. Neurooncol Pract. 2016;3:10–6. https://doi.org/10.1093/nop/npv026.
13. Alexander BM, Cloughesy TF. Adult glioblastoma. J Clin Oncol. 2017;35:2402–9. https://doi.org/10.1200/jco.2017.73.0119.
14. Stupp R, et al. Effect of tumor-treating fields plus maintenance temozolomide vs maintenance temozolomide alone on survival in patients with glioblastoma: a randomized clinical trial. JAMA. 2017;318:2306–16. https://doi.org/10.1001/jama.2017.18718.
15. Weller M, et al. European Association for Neuro-Oncology (EANO) guideline on the diagnosis and treatment of adult astrocytic and oligodendroglial gliomas. Lancet Oncol. 2017;18:e315–29. https://doi.org/10.1016/s1470-2045(17)30194-8.
16. Stupp R, et al. Radiotherapy plus concomitant and adjuvant temozolomide for glioblastoma. N Engl J Med. 2005;352:987–96. https://doi.org/10.1056/NEJMoa043330.
17. Ringel F, et al. Clinical benefit from resection of recurrent glioblastomas: results of a multicenter study including 503 patients with recurrent glioblastomas undergoing surgical resection. Neuro Oncol. 2016;18:96–104. https://doi.org/10.1093/neuonc/nov145.
18. Wu W, et al. Glioblastoma multiforme (GBM): An overview of current therapies and mechanisms of resistance. Pharmacol Res. 2021;171: 105780. https://doi.org/10.1016/j.phrs.2021.105780.
19. Lang F, Liu Y, Chou FJ, Yang C. Genotoxic therapy and resistance mechanism in gliomas. Pharmacol Ther. 2021;228: 107922. https://doi.org/10.1016/j.pharmthera.2021.107922.
20. Li J, et al. Validation and simplification of the Radiation Therapy Oncology Group recursive partitioning analysis classification for glioblastoma. Int J Radiat Oncol Biol Phys. 2011;81:623–30. https://doi.org/10.1016/j.ijrobp.2010.06.012.
21. Stackhouse CT, et al. An in vivo model of glioblastoma radiation resistance identifies long noncoding RNAs and targetable kinases. JCI Insight. 2022. https://doi.org/10.1172/jci.insight.148717.
22. Simon N, Friedman J, Hastie T, Tibshirani R. Regularization paths for Cox's proportional hazards model via coordinate descent. J Stat Softw. 2011;39:1–13. https://doi.org/10.18637/jss.v039.i05.
23. Friedman J, Hastie T, Tibshirani R. Regularization paths for generalized linear models via coordinate descent. J Stat Softw. 2010;33:1–22.
24. Syro LV, et al. Temozolomide and pituitary tumors: current understanding, unresolved issues, and future directions. Front Endocrinol (Lausanne). 2018;9:318. https://doi.org/10.3389/fendo.2018.00318.
25. Kaina B, Ziouta A, Ochs K, Coquerelle T. Chromosomal instability, reproductive cell death and apoptosis induced by O6-methylguanine in Mex-, Mex+ and methylation-tolerant mismatch repair compromised cells: facts and models. Mutat Res. 1997;381:227–41. https://doi.org/10.1016/s0027-5107(97)00187-5.
26. Meikrantz W, Bergom MA, Memisoglu A, Samson L. O6-alkylguanine DNA lesions trigger apoptosis. Carcinogenesis. 1998;19:369–72. https://doi.org/10.1093/carcin/19.2.369.
27. Knizhnik AV, et al. Survival and death strategies in glioma cells: autophagy, senescence and apoptosis triggered by a single type of temozolomide-induced DNA damage. PLoS ONE. 2013;8: e55665. https://doi.org/10.1371/journal.pone.0055665.
28. Aasland D, et al. Temozolomide induces senescence and repression of DNA repair pathways in glioblastoma cells via activation of ATR-CHK1, p21, and NF-κB. Cancer Res. 2019;79:99–113. https://doi.org/10.1158/0008-5472.Can-18-1733.
29. Chakravarti A, et al. Temozolomide-mediated radiation enhancement in glioblastoma: a report on underlying mechanisms. Clin Cancer Res. 2006;12:4738–46. https://doi.org/10.1158/1078-0432.Ccr-06-0596.
30. Hegi ME, et al. MGMT gene silencing and benefit from temozolomide in glioblastoma. N Engl J Med. 2005;352:997–1003. https://doi.org/10.1056/NEJMoa043331.
31. Wu Y, Song Y, Wang R, Wang T. Molecular mechanisms of tumor resistance to radiotherapy. Mol Cancer. 2023;22:96. https://doi.org/10.1186/s12943-023-01801-2.
32. Usui H, Ichikawa T, Miyazaki Y, Nagai S, Kumanishi T. Isolation of cDNA clones of the rat mRNAs expressed preferentially in the prenatal stages of brain development. Brain Res Dev Brain Res. 1996;97:185–93. https://doi.org/10.1016/s0165-3806(96)00152-6.
33. Aikawa S, Kato T, Elsaesser F, Kato Y. Molecular cloning of porcine neuronatin and analysis of its expression during pituitary ontogeny. Exp Clin Endocrinol Diabetes. 2003;111:475–9. https://doi.org/10.1055/s-2003-44706.
34. Joseph R, Dou D, Tsang W. Neuronatin mRNA: alternatively spliced forms of a novel brain-specific mammalian developmental gene. Brain Res. 1995;690:92–8. https://doi.org/10.1016/0006-8993(95)00621-v.
35. Suh YH, et al. Ectopic expression of Neuronatin potentiates adipogenesis through enhanced phosphorylation of cAMP-response element-binding protein in 3T3-L1 cells. Biochem Biophys Res Commun. 2005;337:481–9. https://doi.org/10.1016/j.bbrc.2005.09.078.
36. Dugu L, et al. Neuronatin is related to keratinocyte differentiation by up-regulating involucrin. J Dermatol Sci. 2014;73:225–31. https://doi.org/10.1016/j.jdermsci.2013.10.008.
37. Millership SJ, et al. Neuronatin regulates pancreatic β cell insulin content and secretion. J Clin Invest. 2018;128:3369–81. https://doi.org/10.1172/jci120115.
38. Oyang EL, Davidson BC, Lee W, Poon MM. Functional characterization of the dendritically localized mRNA neuronatin in hippocampal neurons. PLoS ONE. 2011;6: e24879. https://doi.org/10.1371/journal.pone.0024879.
39. Ryu S, et al. Suppression of miRNA-708 by polycomb group promotes metastases by calcium-induced cell migration. Cancer Cell. 2013;23:63–76. https://doi.org/10.1016/j.ccr.2012.11.019.
40. Shinde V, Pitale PM, Howse W, Gorbatyuk O, Gorbatyuk M. Neuronatin is a stress-responsive protein of rod photoreceptors. Neuroscience. 2016;328:1–8. https://doi.org/10.1016/j.neuroscience.2016.04.023.
41. Sharma J, Rao SN, Shankar SK, Satishchandra P, Jana NR. Lafora disease ubiquitin ligase malin promotes proteasomal degradation of neuronatin and regulates glycogen synthesis. Neurobiol Dis. 2011;44:133–41. https://doi.org/10.1016/j.nbd.2011.06.013.
42. Sel S, et al. Temporal and spatial expression pattern of Nnat during mouse eye development. Gene Expr Patterns. 2017;23–24:7–12. https://doi.org/10.1016/j.gep.2016.12.002.

43. Siu IM, et al. Coexpression of neuronatin splice forms promotes medulloblastoma growth. Neuro Oncol. 2008;10:716–24. https://doi.org/10.1215/15228517-2008-038.
44. Pitale PM, Howse W, Gorbatyuk M. Neuronatin protein in health and disease. J Cell Physiol. 2017;232:477–81. https://doi.org/10.1002/jcp.25498.
45. Kanno N, Fujiwara K, Yoshida S, Kato T, Kato Y. Dynamic changes in the localization of neuronatin-positive cells during neurogenesis in the embryonic rat brain. Cells Tissues Organs. 2019;207:127–37. https://doi.org/10.1159/000504359.
46. Ka HI, et al. Neuronatin is associated with an anti-inflammatory role in the white adipose tissue. J Microbiol Biotechnol. 2017;27:1180–8. https://doi.org/10.4014/jmb.1702.02049.
47. Mzhavia N, et al. Neuronatin: a new inflammation gene expressed on the aortic endothelium of diabetic mice. Diabetes. 2008;57:2774–83. https://doi.org/10.2337/db07-1746.
48. Joseph RM. Neuronatin gene: imprinted and misfolded: studies in Lafora disease, diabetes and cancer may implicate NNAT-aggregates as a common downstream participant in neuronal loss. Genomics. 2014;103:183–8. https://doi.org/10.1016/j.ygeno.2013.12.001.
49. Gu T, Su X, Zhao S, Li C. Methylation differences of the neuronatin gene promoter region in liver between normal and cloned pigs. Anim Genet. 2014;45:122–4. https://doi.org/10.1111/age.12074.
50. Hubertus J, et al. Selective methylation of CpGs at regulatory binding sites controls NNAT expression in Wilms tumors. PLoS ONE. 2013;8:e67605. https://doi.org/10.1371/journal.pone.0067605.
51. Yokota N, et al. Identification of differentially expressed and developmentally regulated genes in medulloblastoma using suppression subtraction hybridization. Oncogene. 2004;23:3444–53. https://doi.org/10.1038/sj.onc.1207475.
52. Tajiri T, et al. Classification of neuroblastomas based on an analysis of the expression of genes related to prognosis. J Pediatr Surg. 2007;42:2046–9. https://doi.org/10.1016/j.jpedsurg.2007.08.024.
53. Higashi M, et al. High expressions of neuronatin isoforms in favorable neuroblastoma. J Pediatr Hematol Oncol. 2007;29:551–6. https://doi.org/10.1097/MPH.0b013e3181256b7b.
54. Saeed H, et al. Aberrant epigenetic silencing of neuronatin is a frequent event in human osteosarcoma. Oncotarget. 2020;11:1876–93. https://doi.org/10.18632/oncotarget.27583.
55. Deng Y, et al. DNA methylation-mediated silencing of Neuronatin promotes hepatocellular carcinoma proliferation through the PI3K-Akt signaling pathway. Life Sci. 2023;312: 121266. https://doi.org/10.1016/j.lfs.2022.121266.
56. Thelin-Järnum S, Lassen C, Panagopoulos I, Mandahl N, Aman P. Identification of genes differentially expressed in TLS-CHOP carrying myxoid liposarcomas. Int J Cancer. 1999;83:30–3. https://doi.org/10.1002/(sici)1097-0215(19990924)83:1%3c30::aid-ijc6%3e3.0.co;2-4.
57. Okubo C, et al. Analysis of differentially expressed genes in neuroendocrine carcinomas of the lung. J Thorac Oncol. 2006;1:780–6.
58. Uchihara T, et al. Neuronatin expression and its clinicopathological significance in pulmonary non-small cell carcinoma. J Thorac Oncol. 2007;2:796–801. https://doi.org/10.1097/JTO.0b013e318145af5e.
59. Plasterer C, et al. Neuronatin is a modifier of estrogen receptor-positive breast cancer incidence and outcome. Breast Cancer Res Treat. 2019;177:77–91. https://doi.org/10.1007/s10549-019-05307-8.
60. Kuerbitz SJ, Pahys J, Wilson A, Compitello N, Gray TA. Hypermethylation of the imprinted NNAT locus occurs frequently in pediatric acute leukemia. Carcinogenesis. 2002;23:559–64. https://doi.org/10.1093/carcin/23.4.559.
61. Xu DS, et al. Neuronatin in a subset of glioblastoma multiforme tumor progenitor cells is associated with increased cell proliferation and shorter patient survival. PLoS ONE. 2012;7: e37811. https://doi.org/10.1371/journal.pone.0037811.
62. Bach LA. Recent insights into the actions of IGFBP-6. J Cell Commun Signal. 2015;9:189–200. https://doi.org/10.1007/s12079-015-0288-4.
63. Seurin D, Lassarre C, Bienvenu G, Babajko S. Insulin-like growth factor binding protein-6 inhibits neuroblastoma cell proliferation and tumour development. Eur J Cancer. 2002;38:2058–65. https://doi.org/10.1016/s0959-8049(02)00240-x.
64. Zhao C, et al. Decreased expression of IGFBP6 correlates with poor survival in colorectal cancer patients. Pathol Res Pract. 2020;216: 152909. https://doi.org/10.1016/j.prp.2020.152909.
65. Yang Z, Bach LA. Differential effects of insulin-like growth factor binding protein-6 (IGFBP-6) on migration of two ovarian cancer cell lines. Front Endocrinol (Lausanne). 2014;5:231. https://doi.org/10.3389/fendo.2014.00231.
66. Chen Q, et al. IGFBP6 is a novel nasopharyngeal carcinoma prognostic biomarker. Oncotarget. 2016;7:68140–50. https://doi.org/10.18632/oncotarget.11886.
67. Zhang S, et al. MAFB promotes the malignant phenotypes by IGFBP6 in esophageal squamous cell carcinomas. Exp Cell Res. 2022;416: 113158. https://doi.org/10.1016/j.yexcr.2022.113158.
68. Zong Z, Xin L, Tang X, Guo H. The clinical characteristics and prognostic value of IGFBP6 in glioma. Neurol Res. 2022;44:113–20. https://doi.org/10.1080/01616412.2021.1963620.
69. Bei Y, et al. IGFBP6 regulates cell apoptosis and migration in glioma. Cell Mol Neurobiol. 2017;37:889–98. https://doi.org/10.1007/s10571-016-0426-4.
70. Zhong Z, Xu X, Han S, Shao Y, Yi Y. Comprehensive analysis of prognostic value and immune infiltration of IGFBP family members in glioblastoma. J Healthc Eng. 2022;2022:2929695. https://doi.org/10.1155/2022/2929695.
71. Longhitano L, et al. Lactate modulates microglia polarization via IGFBP6 expression and remodels tumor microenvironment in glioblastoma. Cancer Immunol Immunother. 2023;72:1–20. https://doi.org/10.1007/s00262-022-03215-3.
72. Ma Y, Xi Z. Integrated analysis of multiomics data identified molecular subtypes and oxidative stress-related prognostic biomarkers in glioblastoma multiforme. Oxid Med Cell Longev. 2022;2022:9993319. https://doi.org/10.1155/2022/9993319.
73. Oliva CR, et al. IGFBP6 controls the expansion of chemoresistant glioblastoma through paracrine IGF2/IGF-1R signaling. Cell Commun Signal. 2018;16:61. https://doi.org/10.1186/s12964-018-0273-7.
74. Reeder BJ. Insights into the function of cytoglobin. Biochem Soc Trans. 2023;51:1907–19. https://doi.org/10.1042/bst20230081.
75. Bholah TC, Neergheen-Bhujun VS, Hodges NJ, Dyall SD, Bahorun T. Cytoglobin as a biomarker in cancer: potential perspective for diagnosis and management. Biomed Res Int. 2015;2015: 824514. https://doi.org/10.1155/2015/824514.
76. Shivapurkar N, et al. Cytoglobin, the newest member of the globin family, functions as a tumor suppressor gene. Cancer Res. 2008;68:7448–56. https://doi.org/10.1158/0008-5472.Can-08-0565.

77. Oleksiewicz U, Liloglou T, Field JK, Xinarianos G. Cytoglobin: biochemical, functional and clinical perspective of the newest member of the globin family. Cell Mol Life Sci. 2011;68:3869–83. https://doi.org/10.1007/s00018-011-0764-9.
78. Chen H, Zhao X, Meng T. Expression and biological role of cytoglobin in human ovarian cancer. Tumour Biol. 2014;35:6933–9. https://doi.org/10.1007/s13277-014-1941-x.
79. Emara M, Salloum N, Allalunis-Turner J. Expression and hypoxic up-regulation of neuroglobin in human glioblastoma cells. Mol Oncol. 2009;3:45–53. https://doi.org/10.1016/j.molonc.2008.11.002.
80. Emara M, Turner AR, Allalunis-Turner J. Hypoxic regulation of cytoglobin and neuroglobin expression in human normal and tumor tissues. Cancer Cell Int. 2010;10:33. https://doi.org/10.1186/1475-2867-10-33.
81. Fang J, Ma I, Allalunis-Turner J. Knockdown of cytoglobin expression sensitizes human glioma cells to radiation and oxidative stress. Radiat Res. 2011;176:198–207. https://doi.org/10.1667/rr2517.1.
82. Liu Y, et al. Expression characteristics and their functional role of IGFBP gene family in pan-cancer. BMC Cancer. 2023;23:371. https://doi.org/10.1186/s12885-023-10832-3.
83. Wang J, et al. Identification of immune cell infiltration and diagnostic biomarkers in unstable atherosclerotic plaques by integrated bioinformatics analysis and machine learning. Front Immunol. 2022;13: 956078. https://doi.org/10.3389/fimmu.2022.956078.
84. Liu R, Hu Y, Liu T, Wang Y. Profiles of immune cell infiltration and immune-related genes in the tumor microenvironment of osteosarcoma cancer. BMC Cancer. 2021;21:1345. https://doi.org/10.1186/s12885-021-09042-6.

Publisher's Note Springer Nature remains neutral with regard to jurisdictional claims in published maps and institutional affiliations.